Original Article
Food Science and Technology

ISSN 0101-2061 (Print)
ISSN 1678-457X (Online)

DOI: https://doi.org/10.1590/fst.40421



# Comparative studies on the structure, biological activity and molecular mechanisms of polysaccharides from *Craterellus cornucopioide* (CC-M) and *Dictyophora indusiata* (Vent.ex Pers) Fisch (DI-Z)

Xiang DING[1,2], Miao ZHU[1], Yiling HOU[1,3]*

**Abstract**

In this study, two new polysaccharides were extracted from the fruiting bodies of *Craterellus cornucopioide* and *Dictyophora indusiata (Vent.ex Pers) Fisch,* respectively. The results showed that CC-M was composed of Xyl: Glc: Gal in a ratio of 2:5:4. The CC-M takes 1,6-glucose and 1,6-galactose as skeletons, extends a branched chain from galactose 2-O to connect 1,3,4-xylose, and connects β-4-glucose terminal monosaccharide to xylose. DI-Z was also composed of Xyl: Glc: Gal in the ratio of 2:6:5, which takes 1,6-glucose and 1,6-galactose as skeletons, extends a branched chain from galactose 2-O to connect 1,4-xylose and β-4-glucose as terminal group. The results of immunoactivity showed that CC-M and DI-Z have the proliferation activity of B cells, T cells and RAW264.7 cells in vitro, and the effect of CC-M on the proliferation of immune cells was higher than that of DI-Z. In addition, CC-M could significantly promote the secretion of TNF - α, IL-6, IL-1 β, IL-10 and CD163 and enhance the phagocytic ability of RAW264.7 cells. The results of RNA-sequencing showed that CC-M exerted its proliferative activity and immunoregulatory activity on RAW264.7 cells through the interaction of MAPK signaling pathway, NOD like receptor signaling pathway, PI3K-Akt signaling pathway and NF-κB signaling pathway.

**Keywords:** *Craterellus cornucopioide*; *Dictyophora indusiata* (Vent.ex Pers) Fisch; structure identification; immune activity; molecular mechanism.

**Practical Application:** Polysaccharides can be used as a candidate medicine for immunomodulator.

## 1 Introduction

Cancer threatens human health because of its high mortality rate (Hanahan & Weinberg, 2000). Although therapeutic medicines and means are being updated and optimized, the side effects of these conventional therapies cause a series of adverse reactions (Korfage et al., 2007; Evans & McLeod, 2003). Therefore, anti-cancer medicines with good effects and low toxicity are urgently needed. In recent years, natural polysaccharides have received increasing attention in the biomedical field, because they not only have significant anti-tumor and immunomodulatory activities, but also have low toxic side effects (Ding et al., 2012a, b). Fungal polysaccharide is a class of physiologically active macromolecular natural products, usually compose of 10 or more monosaccharide units, and are one of the important substances involved in the growth and development of the body and various life activities (Du et al., 2019; Kumar, 2000). Glucan from *Lentinus edodes* (Berk.) sing had significant anti-tumor activity, and was successfully developed as an anti-tumor drug through clinical trials (Goodridge et al., 2009; Chihara et al., 1969). Since then, polysaccharides from edible fungi have been reported to have other functions, such as antioxidant, antiviral, anti-inflammatory, hypoglycemic, etc. (Ramberg et al., 2010; Su et al., 2019).

*Craterellus cornucopioide* and *Dictyophora indusiata* (Vent.ex Pers) Fisch are two kinds of rare edible and medicinal fungus with high medicinal value . In recent years, studies have shown that polysaccharide from *Craterellus cornucopioide* and *Dictyophora indusiata* (Vent.ex Pers) Fisch have some interesting biological activities, such as bacteriostasis, antioxidation etc. (Yang et al., 2018; Guo et al., 2019; Habtemariam, 2019). However, there are some differences in the structure of polysaccharides from different regions, and there is no report on the study of the polysaccharides of *Craterellus cornucopioide* and *Dictyophora indusiata (Vent.ex Pers) Fisch* from Qingjiang county of Sichuan Province. (China). In the present study, two novel water-soluble polysaccharide CC-M and DI-Z were extracted, isolated and purified from the fruiting bodies of *Craterellus cornucopioide* and *Dictyophora indusiata* (Vent.ex Pers) Fisch, respectively. The chemical structure and immune activity of the two polysaccharides were first studied and compared to help determine the molecular mechanism underlying the biological activity of polysaccharide CC-M and DI-Z.

## 2 Materials and methods

### *2.1 Experimental materials and chemicals*

*Craterellus cornucopioide* and *Dictyophora indusiata* (Vent.ex Pers) Fisch were collected from Qingjiang county of Sichuan Province. (China). The ethanol was purchased from

*Received 07 June, 2021*
*Accepted 15 June, 2021*
[1] *Key Laboratory of Southwest China Wildlife Resources Conservation, College of Life Sciences, China West Normal University, Sichuan, Nanchong, China*
[2] *College of Environmental Science and Engineering, China West Normal University, Sichuan, Nanchong, China*
[3] *Irradiation Preservation Technology Key Laboratory of Sichuan Province, Sichuan Institute of Atomic Energy, Chengdu, Sichuan, China*
*Corresponding author: starthlh@126.com

Swancor Shanghai Fine Chemical Co., Ltd. (Shanghai, China). Trifluoroacetic acid (TFA), standard monosaccharide and dextran of different molecular weight were purchased from Tianjin Kermel Chemical Reagent Co., Ltd. (Tianjin, China). DEAE-cellulose (DE-52) was purchased from Beijing Solarbio Science & Technology Co., Ltd. (Beijing, China). Cell counting kit (CCK-8 cell counting kit) was purchased from Dojindo Molecular Technologies, Inc. (Shanghai, China). PBS buffer, lipopolysaccharide (LPS), 0.5% Trypsin-EDTA, neutral red and dimethyl sulfoxide (DMSO) were purchased from Sigma-Aldrich Inc. (Missouri, USA). RPMI1640 medium (phenol red free) and fetal bovine serum (FBS) were purchased from Gibco Inc. (New York, USA). All analytical reagents were of analytical grade.

### *2.2 Extraction and purification of polysaccharides*

Dry fruiting bodies powder (400 g) was boiled in water for 3 times (6 h for each). The supernatant was concentrated after centrifugation. Three times volume of 95% ethanol were added in the supernatant to precipitate crude polysaccharides. The crude polysaccharides were purified by DEAE cellulose (DE-52) column and dialysis (7000 Da, Biosharp), drying in vacuum freeze-drying machine (ALPHA2-4LD plus, Christ). The final polysaccharide from *Craterellus cornucopioide* and *Dictyophora indusiata* (Vent.ex Pers) Fisch were named CC-M and DI-Z, respectively.

### *2.3 Determination of the molecular weight*

The molecular weight of polysaccharide was determined via high-performance gel permeation chromatography (HPGPC). A total of 10 mg polysaccharide was weighted, dissolved in 1 mL distilled water and filtered (0.22μm pore). The measured data was analyzed via Empower Pro GPC software (version B.01.02; Agilent Technologies Inc., USA) and known dextran standards were used as references.

### *2.4 Fourier Transform Infrared Spectrometer (FT-IR) analysis*

A total of 5 mg polysaccharide was weighted, then ground and mixed with dry KBr (Kamnev et al., 2018). The data was collected via the mixture scanning within 4000 $cm^{-1}$ to 400 $cm^{-1}$ in the fourier transform infrared spectrometer (Nicolet 5700, Thermo Scientific).

### *2.5 Monosaccharide composition analysis*

The monosaccharide composition of polysaccharide was analyzed by high performance liquid chromatography (HPLC) (Agilent 1100, USA), respectively. A total of 20 mg polysaccharide was dissolved in 5 mL trifluoroacetic acid (TFA) solution (2 mol/L) and hydrolyzed for 6 h (100 °C). The supernatant was dried and washed with distilled water to remove residual TFA (repeated 3 times). Operating conditions were detector: RID detector; injection volume: 10 μL; column temperature: 35 °C. Known monosaccharide samples were used as standards.

### *2.6 Methylation analysis and GC-MS*

Methyl iodide reagent was used to obtain methylated polysaccharide. The dry methylated product was dissolved in 2M TFA, then hydrolyzed for 6 h (100 °C). Silane reagent was was used to prepare derivatized product detected by GC-MS (Agilent 7890A, USA). The initial temperature set at 80 °C and maintained for 3 min, with a linear increase to 200 °C at a rate of 10 °C/min, then maintaining at 200 °C for 10 min.

### *2.7 Nuclear Magnetic Resonance (NMR) assay*

A total of 50 mg polysaccharide was dissolved in 500 μl $D_2O$ (Leeuwen et al., 2014). The $^1H$ NMR spectra, $^{13}C$ NMR spectra, $^1H$-$^1H$ COSY spectra, HMQC spectra and HMBC spectra were analyzed by the Varian Unity INOVA 400/45 (Varian Medical Systems, USA) and internal standard was tetramethylsilane.

### *2.8 Cell lines and reagents*

Macrophages RAW264.7 cell line, B cell line, T cell line and S180 cell line (sarcoma cell) were purchased from the cell bank of the Typical Culture Preservation Committee of the Chinese Academy of Science (Shanghai, China). All cells were cultivated in RPMI 1640 medium with 10% FBS, 1% penicillin (100 IU/mL) and streptomycin (100 mg/L) at 37 °C with 5% $CO_2$. All cell lines came from mice.

### *2.9 T cells, B cells and RAW264.7 cells proliferation assay*

Pharmacological evaluation of polysaccharide on T cells, B cells and RAW264.7 cells proliferation was examined via CCK-8 method. Cells ($1x10^5$ cells/mL) were added to a 96-well plate (100 μL/well) and incubated for 24 h (5% $CO_2$, 37 °C). Different concentrations of polysaccharide (final concentration 5, 10, 20 μg/mL) were added to the 96-well plate (100 μL/well), incubated for 24 h. LPS (final concentration 5 μg/mL) and the cell culture medium were used as positive control and negative control, respectively. Proliferation assay was analyzed via instructions of CCK-8. The value of optical density (OD) was detected at 450 nm. The way of calculating cell viability was: cell proliferation rate (%) = [(As-Ac)/(Ac-Ab)] × 100%, where Ac was the absorbance of negative control group, Ab was the absorbance of blank group, As was the absorbance of experimental groups. The Leica Microsystems inverted fluorescence microscope (DMI4000B, Germany) was used to observe the cell morphology and alterations to cell numbers.

### *2.10 Pharmacological evaluation for macrophage phagocytic activity of neutral red reagent*

RAW264.7 cells ($1 \times 10^5$ cells/mL) were seeded into 96-well plates at 100 μL/well and incubated for 24 h. Subsequently, 100 μL cell culture medium (blank control), LPS (final concentra-tion 5 μg/mL, positive control) and CC-M solutions (5, 10 and 20 μg/mL) were added to the 96-well plates. After incubation at 37 °C for 24 h, neutral red reagent (0.075 g/L) was added to the 96-well plates. After 30 min, the neutral red reagent was discarded and the cells were washed with PBS thrice, followed by the addition of 200 μL lysis buffer (ethanol:glacial acetic acid, 1:1).

The 96-well plates were placed in an incubator for 2 h. The OD was measured at 540 nm.

### *2.11 Pharmacological evaluation for macrophage phagocytic activity of fluorescent microsphere*

RAW264.7 cells ($1 \times 10^5$ cells/mL) were seeded into 96-well plates at 100 μL/well and incubated for 24 h, and then 200 μL fluorescent microsphere diluent with a concentration of $1 \times 10^7$ / ml was added to each well. The cell culture plate was wrapped with tin foil and incubated at 37 °C for 2 h; After incubation, the diluent of fluorescent microspheres was discarded, and PBS buffer was added to clean the microspheres for three times. Add 200 μL cell lysate (anhydrous ethanol: glacial acetic acid = 1:1) into each well of 96 well plate to dry PBS solution, and lyse at 37 °C in dark for 15 min. Measure the absorbance value of each well with at 505 nm.

### *2.12 Evaluating cytokine levels*

In order to understand the alterations in the level of cytokines of TNF-α, IL-6, IL-10, IL-1β and CD163, ELISA kits were used according to the manufacturers' protocols.

### *2.13 Transcriptome sequencing*

The collected cells of control group, LPS group and CC-M group were used to carry out transcriptome assay. The cells, quickly freezed by liquid nitrogen, were sent to Novogene Bioinformatics Technology Co. Ltd, Beijing, China. The remaining tumor tissues were stored at -80 °C. After the samples were quantified, the library was constructed and checked, and subsequently sequenced using an Illumina Hiseq platform . Genes with an adjusted $P < 0.05$ identified by DESeq2 were classified as differentially expressed. Subsequently, the clusterProfiler R package was used for Gene Ontology (GO) analysis and Kyoto Encyclopedia of Genes and Genomes (KEGG) pathways analysis. Differentially expressed genes were analyzed using the edgeR program (version 3.11) (Cock et al., 2010).

### *2.14 Statistical analysis*

Data were showed as the mean ± standard deviation (SD). All statistical comparisons were analyzed using a one-way analysis of variance (ANOVA) test followed by StudentNewmanKeuls test with SPSS 17.0 software. Compared with the blank control group, the significant difference was indicated by *, $P < 0.05$, and the extremely significant difference was indicated by * *, $P < 0.01$.

## 3 Results and discussion

### *3.1 Elution curve of polysaccharide*

Distilled water, 0.05 mol/l, 0.1 mol/l and 0.2 mol/l NaCl were used as eluents to elute polysaccharide from *Craterellus cornucopioide* and *Dictyophora indusiata* (Vent.ex Pers) Fisch, respectively. The elution results of polysaccharide were shown in Figure 1A, 1B. With the increase of NaCl concentration, there are four and one main elution peaks, respectively. In this study, all neutral polysaccharide eluates in distilled water were collected as the research objects. According to the calculation, the yield of CC-M and DI-Z in the total fruiting body were about 0.5% and 0.3%, respectively.

### *3.2 Molecular weight of polysaccharides*

The molecular weight of polysaccharide was determined by HPGPC. The weight-average molecular weight (Mw) was 20 482 Da, the peak molecular weight (Mp) was 17 894 Da, the number-average molecular weight (Mn) was 11 369 Da and the polydispersity was 1.80 of polysaccharides CC-M (Figure 1C). The weight-average molecular weight (Mw) was 9 779 Da, the peak molecular weight (Mp) was 11 830 Da, the number-average molecular weight (Mn) was 2 587 Da and the polydispersity was 3.78 of polysaccharides DI-Z (Figure 1D).

### *3.3 FT-IR analysis of polysaccharides*

In this study, FT-IR was used to determine the infrared absorption spectra of CC-M and DI-Z in the range of 4000-400 $cm^{-1}$. The results of CC-M infrared spectrum were shown in Figure 1E. A strong and broad absorption peak at 3436.02 $cm^{-1}$ was assigned to the OH stretching vibration. The band at 2922.70 $cm^{-1}$and 2853.44 $cm^{-1}$ were designated as CH stretching vibration peak of $-CH_2$ and $-CH_3$, respectively. The next band at 1633.45 $cm^{-1}$ was due to C=O deformation vibration. The absorption peak at 1401.69 $cm^{-1}$ was caused by bending vibration peak of CH. The peak at 1096.00 $cm^{-1}$ can be classified as C-O stretching vibration, and the peak at 553.46 $cm^{-1}$ can be classified as C-H rocking vibration.

The results of DI-Z infrared spectrum were shown in Figure 1F. The strong and broad absorption peak at 3430.76 $cm^{-1}$ was assigned to the OH stretching vibration. The band at 2922.93 $cm^{-1}$ and 2 854.18 $cm^{-1}$ were designated as CH stretching vibration peak of $-CH_2$ and $-CH_3$, respectively. The next band at 1633.46 $cm^{-1}$ was due to C=O deformation vibration. The absorption peak at 1399.64 $cm^{-1}$ was caused by bending vibration peak of CH. The peak at 1127.04 $cm^{-1}$ can be classified as C-O stretching vibration. These results indicate that CC-M and DI-Z are a kind of polysaccharide with the characteristics of polysaccharide infrared spectrum.

### *3.4 Monosaccharide composition analysis of polysaccharides*

The results of HPLC could directly reflect the composition and ratio of monosaccharides of the polysaccharide. The corresponding retention time of the standards was 4.322 min for Rha, 4.960 min for Xyl, 5.643 min for Ara, 6.725 min for Glc and 7.266 min for Gal. Compared with the peak retention time of the monosaccharide standard, there were three retention time peaks in the HPLC results of CC-M, namely Xyl represented by the retention time of 5.066 min, Glc represented by the retention time of 6.716 min and Gal represented by the retention time of 7.249 min. The ratio of Xyl: Glc: Gal in CC-M was determined to be around 2:5:4 based on the area ratio of the three peaks. And there were also three retention time peaks in the HPLC results of DI-Z, Xyl represented by the retention time of 5.053 min, Glc represented by the retention time of 6.457 min and Gal

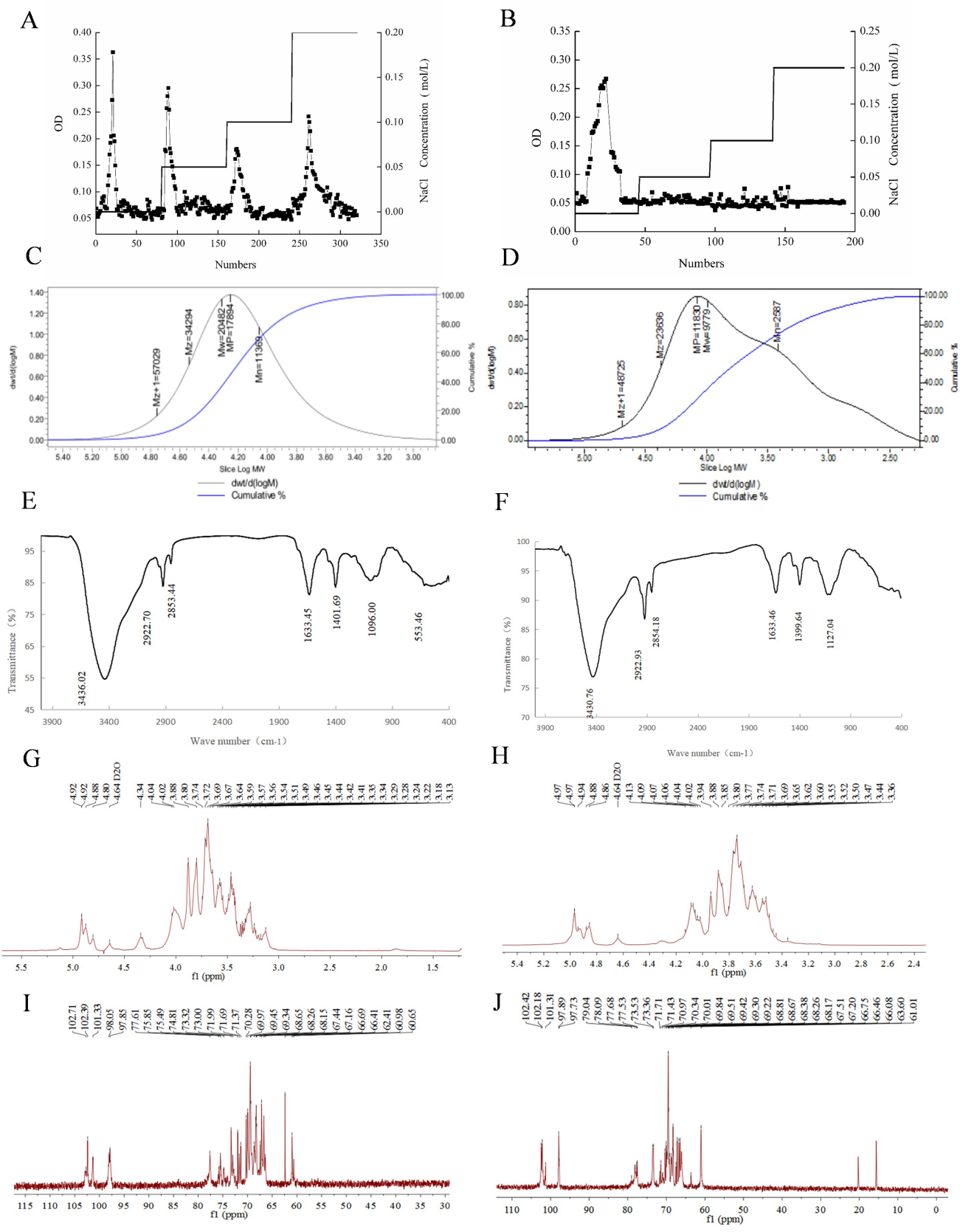


**Figure 1**. (A) Elution curve of CC-M by column chromatography; (B) Elution curve of DI-Z by column chromatography; (C) The molecular weight of CC-M; (D) The molecular weight of DI-Z; (E) The fourier transform infrared spectra of CC-M; (F) The fourier transform infrared spectra of DI-Z; (G) The $^{1}$H NMR spectra of CC-M; (H) The $^{1}$H NMR spectra of DI-Z; (I) The $^{13}$C NMR spectra of CC-M; (J) The $^{13}$C NMR spectra of DI-Z.

represented by the retention time of 7.247 min. The ratio of them in DI-Z was determined to be about 2:6:5.

### *3.5 GC-MS analysis of polysaccharides*

The connection site of polysaccharides was determined by GC-MS. The GCMS results showed that the data of fragment ion peaks of CC-M conformed to the Dconfiguration monosaccharide fragment ion peaks. Thus, the Dconfiguration was the configuration of xylose, glucose and galactose residues in CC-M. In this study, the results showed that the D-xylopyranose residues were 2,6-di-O-methyl-1,3,4-tris-O-trimethysilyl-substituted, D-glucosepyranose residues were 2,3,4-tri-O-methyl-1,6-bis-O-trimethysilyl-substitued and 1,2,3,6-tri-O-methyl-4-bis-O-trimethysilyl-substitued, and D-galactopyranose residues were 3,4-di-O-methyl-1,2,6-tris-O-trimethysilyl-substituted and 2,4-di-O-methyl-1,3,6-tris-O-trimethysilyl-substituted (Table 1). Furthermore, the ratio of Xyl: Glc: Gal in CC-M was approximately 2:5:4, which was consistent with the results of HPLC. In accordance with FT-IR, monosaccharide composition and methylation results of CC-M, it was inferred that CC-M takes 1,6-glucose and 1,6-galactose as skeletons, extends a branched chain from galactose 2-O to connect 1,3,4-xylose, and connects β-4-glucose terminal monosaccharide to xylose.

The GCMS results showed that the data of fragment ion peaks of DI-Z also conformed to the Dconfiguration monosaccharide fragment ion peaks. And the Dconfiguration was the configuration of glucose, galactose and xylose residues in DI-Z. The results showed that the D-xylopyranose residues were 3,6-di-O-methyl-1,2,4-tris-O-trimethysilyl-substituted, D-glucosepyranose residues were 2,3,4-tri-O-methyl-1,6-bis-O-trimethysilyl-substitued and 1,2,3,6-tri-O-methyl-4-bis-O-trimethysilyl-substitued, and D-galactopyranose residues was 3,4-di-O-methyl-1,2,6-tris-O-trimethysilyl-substituted (Table 2). The ratio of them was approximately 2:6:5, which was also consistent with the results of HPLC. In accordance with FT-IR, monosaccharide composition and methylation results of DI-Z, it was inferred that DI-Z takes 1,6-glucose and 1,6-galactose as skeletons, extends a branched chain from galactose 2-O to connect 1,4-xylose and β-4-glucose as terminal group.

### *3.6 $^{1}$H-NMR analysis of polysaccharides*

NMR could provide related hydrogen and carbon signals of different monosaccharides in polysaccharides. In the $^{1}$H NMR (400 HZ) spectrum (Figure 1G), signals at δ 4.92, δ 4.92, δ 4.88, δ 4.80 and δ 4.34 signified that CC-M had five anomeric protons, which suggested that CC-M is composed of at least five monosaccharides with different linking modes. The signal peaks of δ 4.92, δ 4.92, δ 4.88 and δ 4.80 indicated that there were polysaccharides with α configuration, and the signal peak of δ 4.34 indicated that there was a polysaccharide with β configuration in CC-M. The peaks at 4.92 ppm were assigned to anomeric hydrogen signals of (1→6)-α-D-Glcp (A) and (1→2,6)-α-D-Galp (B), respectively, the resonances at 4.88 ppm were attributed to 1,6-linked α-D-Galp (C), the resonances at 4.80 ppm were attributed to (1→3,4)-α-D-Xyl (D) and the resonances at 4.34 ppm were attributed to →4)-β-D-Glcp (E). The peaks at δ 3.13-4.04 ppm were composed of a large number of overlapping hydrogen signals, which were attributed to H2-H6 in each monosaccharide.

In the $^{1}$H NMR (400 HZ) spectrum of DI-Z (Figure 1H), signals at δ 4.97, δ 4.97, δ 4.92, δ 4.88 and δ 4.86 showed that DI-Z also had five anomeric protons. The hydrogen signals were all assigned to α-pyranose unit. The peaks at δ 4.97, δ 4.97, δ 4.92, δ 4.88 and δ 4.86 were assigned to anomeric hydrogen signals of →4)-β-D-Glcp (A), (1→6)-α-D-Glcp (B), (1→4)-α-D-Xyl (C), (1→2,6)-α-D-Galp (D), and (1→6)-α-D-Galp (E), respectively. The peaks at δ 3.36-4.13 ppm were composed of a large number of overlapping hydrogen signals, which were attributed to H2-H6 in each monosaccharide.

### *3.7 $^{13}$C-NMR analysis of polysaccharides*

In the $^{13}$C NMR spectra of CC-M (Figure 1I), the inexistence of chemical shift within δ 106-109 ppm indicated no furan rings in CC-M. The signals of δ 102.71, δ 102.39, δ 101.33, δ 97.78 and δ 97.72 were anomeric carbon peaks and assigned to anomeric carbon signals of →4)-β-D-Glcp (E), (1→6)-α-D-Glcp (A), (1→2,6)-α-D-Galp (B), 1,6-linked α-D-Galp (C) and (1→3,4)-α-D-Xyl (D), respectively. The results show that the shifts of δ 102.39, δ 101.33, δ 97.78 and δ 97.72 can be classified as the

**Table 1**. Linkage sites of monosaccharides in CC-M.

| Methylated sugar | Linkage | m/z |
|---|---|---|
| 1,2,6-tris-O-trimethylsilyl-Gal | 1,2,6- | 59 73 89 133 146 159 173 259 345 377 |
| 1,3,6-tris-O-trimethylsilyl-Gal | 1,3,6- | 59 73 89 146 191 231 |
| 1,6-tris-O-trimethylsilyl-Glc | 1,6- | 59 73 88 101 117 133 145 159 185 205 229 287 319 |
| 1,3,4-tris-O-trimethylsilyl-Xyl | 1,3,4- | 59 73 89 101 116 131 146 159 204 217 231 259 |
| 4-O-trimethylsilyl-Glc | 4- | 59 73 85 88 101 116 133 146 159 187 229 261 |

**Table 2**. Linkage sites of monosaccharides in DI-Z.

| Methylated sugar | Linkage | m/z |
|---|---|---|
| 1,2,6-tris-O-trimethylsilyl-Gal | 1,2,6- | 59 73 89 133 146 159 173 259 317 345 377 |
| 1,6-tris-O-trimethylsilyl-Glc | 1,6- | 59 73 88 101 117 133 159 185 205 229 245 287 319 |
| 1,2,4-tris-O-trimethylsilyl-Xyl | 1,2,4- | 59 73 89 101 146 159 191 217 |
| 4-O-trimethylsilyl- Glcp | 4- | 59 73 85 88 101 116 133 146 159 187 229 261 |

anomeric carbon signals of α - monosaccharide, and δ 102.71 can be classified as the anomeric carbon signals of β - monosaccharide, which further proves that CC-M is a polysaccharide composed of α - monosaccharide and β - monosaccharide. The strong chemical signals within δ 80-60 ppm could be attributed to carbon signals of C2-C6 of glucose and galactose.

In the $^{13}C$ NMR spectra of DI-Z (Figure 1J), the signals of δ 102.42, δ 102.18, δ 101.31, δ 97.89 and δ 97.73 were anomeric carbon peaks and assigned to anomeric carbon signals of →4)-β-D-Glcp (A), (1→2,6)-α-D-Galp (D), (1→6)-α-D-Glcp (B), (1→4)-α-D-Xyl (C) and (1→6)-α-D-Galp (E), respectively. The strong chemical signals within δ 80-60 ppm could be attributed to carbon signals of C2-C6 of glucose and galactose.

### *3.8 $^{1}H$-$^{1}H$COSY analysis of polysaccharides*

Each proton signal of monosaccharides in polysaccharides could be obtained by $^{1}H$-$^{1}H$ COSY spectrum. In the $^{1}H$-$^{1}H$ COSY spectrum of CC-M (Figure 2A), the cross signal A (δ 4.92/3.72), B (δ 4.92/3.54), C (δ 4.88/3.44), D (δ 4.80/3.69) and E (δ 4.34/3.18) represented the correlation between H-1 and H-2 of the (1→6)-α-D-Glcp (A), (1→2,6)-α-D-Galp (B), 1,6-linked α-D-Galp (C), (1→3,4)-α-D-Xyl (D) and →4)-β-D-Glcp (E), respectively. Other signals in the $^{1}H$ NMR spectra of CC-M were assigned and listed in Table 3.

In the $^{1}H$-$^{1}H$ COSY spectrum of DI-Z (Figure 2B), the cross signal A (δ 4.97/δ 3.94), B (δ 4.97/δ 3.74), C (δ 4.94/δ 3.62), D (δ 4.88/δ 3.71) and E (δ 4.86/δ 3.69) represented the correlation between H-1 and H-2 of the →4)-β-D-Glcp (A), (1→6)-α-D-Glcp (B), (1→4)-α-D-Xyl (C), (1→2,6)-α-D-Galp (D) and (1→6)-α-D-Galp (E), respectively. Other signals in the $^{1}H$ NMR spectra of DI-Z were assigned and listed in Table 4.

### *3.9 HMQC analysis of polysaccharides*

The direct correlation of carbon and hydrogen signals could be obtained by HMQC spectra. In the HMQC spectrum of CC-M (Figure 2C), the signal A (δ 4.92/δ 102.39), B (δ 4.92/δ 102.33), C (δ 4.88/δ 98.06), D (δ 4.80/δ 97.85) and E (δ 4.34/δ 102.71) represented the correlation between H-1 and C-1 of the (1→6)-α-D-Glcp (A), (1→2,6)-α-D-Galp (B), 1,6-linked α-D-Galp (C), (1→3,4)-α-D-Xyl (D) and →4)-β-D-Glcp (E), respectively. Other signals in the HMQC spectrum of CC-M were assigned and listed in Table 3.

In the HMQC spectrum of DI-Z (Figure 2D), the signal A (δ 4.97/δ 102.42), B (δ 4.97/δ 101.31), C (δ 4.94/δ 97.89), D (δ 4.88/δ 102.18) and E (δ 4.86/δ 97.73) represented the correlation between H-1 and C-1 of the →4)-β-D-Glcp (A), (1→6)-α-D-Glcp (B), (1→4)-α-D-Xyl (C), (1→2,6)-α-D-Galp (D) and (1→6)-α-D-Galp (E), respectively. Other signals in the HMQC spectrum of CC-M were assigned and listed in Table 4.

### *3.10 HMBC analysis of polysaccharides*

HMBC provided a correlation spectrum between carbon and hydrogen separated by two or three bonds. In the HMBC spectrum of CC-M (Figure 2E), the signal (δ 4.92/δ 73.32), signal (δ 4.92/δ 70.28) and signal (δ 4.34/δ 77.61) conformed to the correlation between H-1 and C-3 of the (1→6)-α-D-Glcp (A), (1→2,6)-α-D-Galp (B) and →4)-β-D-Glcp (E). The chemical signal (δ 3.29/δ 75.85) accorded with the correlation between H-4 and C-6 of (1→2,6)-α-D-Galp (B). The signal (δ 3.44/δ 73.32) and signal (δ 4.44/δ 67.16) corresponded to the correlation between H-2 and C-4 and H-5 and C-3 of 1,6-linked α-D-Galp (C), respectively. The signal (δ 3.49/δ 60.65) and signal (δ 3.74/δ 69.45) conformed to the correlation between H-2 and C-4 and H-5 and C-3 of (1→3,4)-α-D-Xyl (D), respectively.

In the HMBC spectrum of DI-Z (Figure 2F), the signal (δ 4.97/δ73.36, δ3.74/δ68.26) conformed to the correlation between H-1/C-3 and H-2/C-4 of the →4)-β-D-Glcp (A), respectively. Signal (δ 4.04/δ 78.09) conformed to the correlation between H-5/C-3 of (1→6)-α-D-Glcp (B), signal (δ 3.71/δ 61.10) conformed to the correlation between H-5/C-2 of (1→4)-α-D-Xyl (C), signal (δ 3.96/δ 102.18) conformed to the correlation between H-5/C-3 of (1→2,6)-α-D-Galp (D), respectively.

**Table 3**. Chemical shifts of 1H and 13C NMR spectra of CC-M.

| Glycosyl residues | Chemical shifts (ppm) | | | | | |
|---|---|---|---|---|---|---|
| | H1/C1 | H2/C2 | H3/C3 | H4/C4 | H5/C5 | H6/C6 |
| α-D-Glc(A) | 4.92/102.39 | 3.54/60.98 | 3.57/73.32 | 3.29/77.61 | 3.35/62.41 | 3.45/74.81 |
| α-D-Gal(B) | 4.92/101.33 | 3.72/60.65 | 3.69/70.28 | 3.29/75.49 | 3.46/66.69 | 3.21/75.85 |
| α-D-Gal(C) | 4.88/98.06 | 3.44/62.41 | 3.45/67.65 | 3.56/73.32 | 4.04/68.65 | -/- |
| α-D-Xyl(D) | 4.80/97.85 | 3.49/66.69 | 3.69/69.45 | 3.41/60.65 | 3.74/68.26 | 3.46/66.69 |
| β-D-Glc(E) | 4.34/102.71 | 3.18/69.45 | 3.56/77.61 | 3.59/73.00 | 3.88/70.28 | 3.51/71.99 |

**Table 4**. Chemical shifts of $^{1}H$ and $^{13}C$ NMR spectra of DI-Z.

| Glycosyl residues | Chemical shifts (ppm) | | | | | |
|---|---|---|---|---|---|---|
| | H1/C1 | H2/C2 | H3/C3 | H4/C4 | H5/C5 | H6/C6 |
| β-D-Glc(A) | 4.97/102.42 | 3.74/67.20 | 3.65/73.36 | 3.80/68.26 | 3.94/69.84 | 3.69/71.43 |
| α-D-Glc(B) | 4.97/101.31 | 3.94/68.81 | 3.74/78.09 | 3.88/69.51 | 4.04/67.51 | 4.13/68.26 |
| α-D-Glc, α-D-Xyl(C) | 4.94/97.89 | 3.62/61.10 | 3.80/67.51 | 3.88/69.51 | 3.71/71.43 | 3.62/73.53 |
| α-D-Gal(D) | 4.88/102.18 | 3.71/68.09 | 3.96/68.19 | 3.77/61.10 | 3.62/73.53 | 3.94/69.84 |
| α-D-Gal(E) | 4.86/97.73 | 3.69/78.18 | 3.74/67.20 | 4.06/66.75 | 3.55/66.46 | 3.85/66.08 |

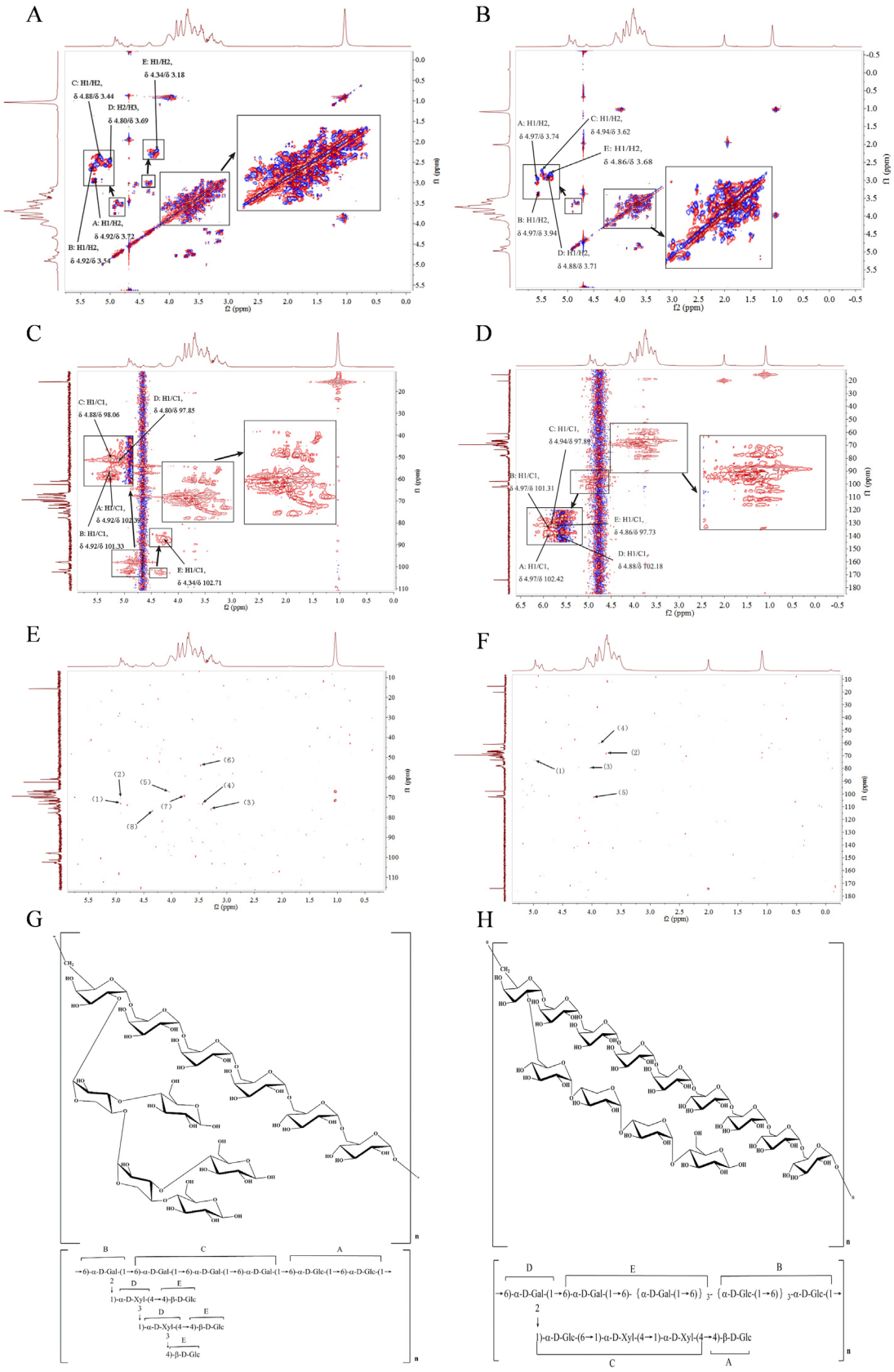


**Figure 2**. (A) $^{1}$H-$^{1}$H COSY spectrum of CC-M; (B) $^{1}$H-$^{1}$H COSY spectrum of DI-Z; (C) HMQC spectrum of CC-M; (D) HMQC spectrum of DI-Z; (E) HMBC spectrum of CC-M; (F) HMBC spectrum of DI-Z; (G) Predicted chemical structure of CC-M; (H) Predicted chemical structure of DI-Z.

The results of structure identification by GC-MS, HPGPC, HPLC, FT-IR and NMR showed that CC-M was composed of Xyl: Glc: Gal in a ratio of 2:5:4. The CC-M takes 1,6-glucose and 1,6-galactose as skeletons, extends a branched chain from galactose 2-O to connect 1,3,4-xylose, and connects β-4-glucose terminal monosaccharide to xylose. DI-Z was also composed of Xyl: Glc: Gal in the ratio of 2:6:5. In accordance with FT-IR, monosaccharide composition and methylation results of DI-Z, it was inferred that DI-Z takes 1,6-glucose and 1,6-galactose as skeletons, extends a branched chain from galactose 2-O to connect 1,4-xylose and β-4-glucose as terminal group. The structure of CC-M and DI-Z were shown in Figure 2G, 2H.

### *3.11 Effect of CC-M and DI-Z on T cell proliferation*

T cells were differentiated from bone marrow stem cells, which could participate in the cellular immunity of the body (Zheng & Flavell, 2016). The analysis of results showed that polysaccharide group of CC-M and DI-Z (final concentration 5, 10, 20 μg/mL, respectively) could significantly promote the proliferation of T cells compared with the blank control group (Figure 3A, 3C). When the concentration of CC-M and DI-Z was 10 μg/mL, the proliferation efficiency of T cells reached the maximum, and was higher than that of the positive control group (LPS was 5 μg/mL). Cell morphology observation demonstrated that compared with cells in blank control group, cells stimulated by CC-M and DI-Z formed large clusters and increased in number (Figure 3B, 3D).

### *3.12 Effect of CC-M and DI-Z on proliferation of B cells*

B cells were derived from the pluripotent stem cells of bone marrow, which could proliferate and differentiate into a large number of plasma cells when stimulated by antigens. Plasma cells could synthesize and secrete antibodies in the blood circulation, which plays an important role in the development and regulation of the immune system (Brown et al., 2004). The results indicated that when the final mass concentration of polysaccharide was 5-20 μg/ml, the proliferation effect of B cells was enhanced. When the final concentration of CC-M and DI-Z was 10 μg/ml, the effect of promoting B cell proliferation was the best, which was significantly different from that of the blank control group ($P < 0.01$) (Figure 3E, 3G). The morphology of polysaccharide stimulated B cell was shown in Figure 3F, 3H. B cells grew well, mostly round, and grew in clusters. When polysaccharide was increased, the number of cells and the volume of cell colony also increased.

### *3.13 Effect of CC-M on proliferation of RAW264.7 cells*

RAW264.7 cells has a variety of immune functions and strong ability of adhesion and phagocytosis of antigens. They could not only participate in innate immunity of the body, but also play an

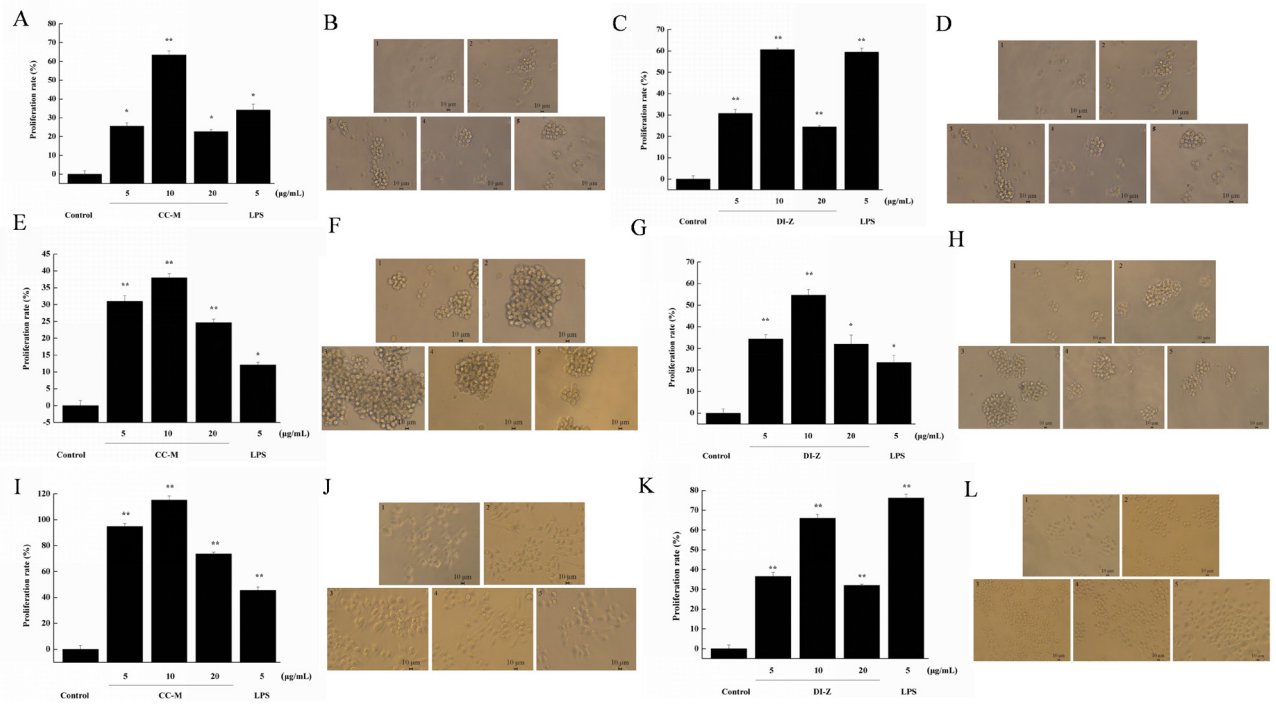


**Figure 3**. (A) Effect on the proliferation of T cells by CC-M; (B) Effect on T cells morphology by CC-M; (C) Effect on the proliferation of T cells by DI-Z; (D) Effect on T cells morphology by DI-Z; (E) Effect on the proliferation of B cells by CC-M; (F) Effect on B cells morphology by CC-M; (G) Effect on the proliferation of B cells by DI-Z; (H) Effect on B cells morphology by DI-Z; (I) Effect on the proliferation of RAW264.7 cells by CC-M; (J) Effect on RAW264.7 cells morphology by CC-M; (K) Effect on the proliferation of RAW264.7 cells by DI-Z; (L) Effect on RAW264.7 cells morphology by DI-Z. 1 was the control group, 2-4 was the experimental group, and the mass concentrations were 2.5, 5, 10 μg/mL, and 5 was the LPS positive control group (5 μg/mL). Compared with the control group, the difference was significant ($P < 0.05$) expressed by * and very significant ($P < 0.01$) expressed by **.

important role in immune regulation by participating in acquired immunity (Yeo et al., 2003). As shown in Figure 3I, 3K, when the final mass concentration of polysaccharide was 5-20 μg/ml, the proliferation effect of RAW264.7 cells increases with the increase of different concentrations of polysaccharide. When the final concentration of CC-M and DI-Z was 10 μg/ml, the proliferation rate of RAW264.7 cells was significantly higher than that of the blank control group ($P < 0.01$). The proliferation morphology of RAW264.7 cells stimulated by CC-M and DI-Z were shown in Figure 3J, 3L. RAW264.7 macrophage was in the state of high refraction circle and part of cells extend pseudopodia, and adheres to the wall under the stimulation of polysaccharide CC-M and DI-Z.

### *3.14 Effect of CC-M on phagocytic function of RAW264.7 cells by neutral red*

The results showed that CC-M had very good immunostimulatory activity on macrophages (Figure 4A). In the next experiment, the immune activity of CC-M on macrophages was further explored. Macrophages belong to phagocytes, and their ability to phagocyte reflects the level of immune system. Neutral red is a fluorescent reagent with high molecular weight and can only enter macrophages through phagocytosis. Neutral red assay was used to evaluate whether CC-M could enhance the phagocytic activity of RAW264.7 cells. Compared with the blank control group, when the final concentration of CC-M was 5-20 μg/ml, the phagocytic ability of RAW264.7 cells was significantly enhanced ($P < 0.01$). When the final concentration of CC-M was 20 μg/ml, the phagocytic ability of RAW264.7 cells was lower than that when the final concentration of CC-M was 5-10 μg/ml. In conclusion, the optimal concentration of CC-M to stimulate RAW264.7 cells to phagocytize neutral red was 10μg/ml, and the phagocytic rate was 66.27%. At the concentration of 5 μg/ml, the phagocytic rate of RAW264.7 cells stimulated by CC-M (39.57%) was higher than that of LPS positive control group (24.88%). These results further indicate that CC-M can not only significantly stimulate the proliferation of RAW264.7, but also significantly enhance the phagocytic function of RAW264.7, which plays an important role in activating the immune system and maintaining the homeostasis of the environment.

### *3.15 Effect of CC-M on phagocytosis of RAW264.7 cells by fluorescent microspheres*

The effect of polysaccharide CC-M on the phagocytic ability of RAW264.7 cells to fluorescent microspheres is shown in Figure 4B, 4C. Compared with the blank control group, when the concentration of CC-M is 5, 10 and 20 μg/ml, the phagocytic rates of cells phagocytizing fluorescent microspheres are 64.84%, 79.71% and 61.83%, respectively. When the concentration of CC-M was 10 μg/ml, the phagocytic rate of RAW264.7 cells was the highest. These results indicate that CC-M can promote the phagocytosis of RAW264.7 to different foreign bodies, and the optimal phagocytic concentration is the same as the neutral red experiment. However, the highest phagocytic rate is different due to different experimental subjects of phagocytosis. The morphological observation of phagocytosis of RAW264.7 cells was shown in Figure 4C. When the concentration of CC-M was 10 μg/ml, compared with the blank control group, the phagocytosis of RAW264.7 cells on the fluorescent microspheres under stimulation of CC-M was significantly increased.

### *3.16 Effect of CC-M on cytokines secreted by RAW264.7 cells*

After RAW264.7 cells were stimulated with CC-M and LPS for 24 h, the secretion of TNF-α, IL-6, IL-1 β, IL-10 and CD163 was detected by ELISA. The standard curves of TNF - α,

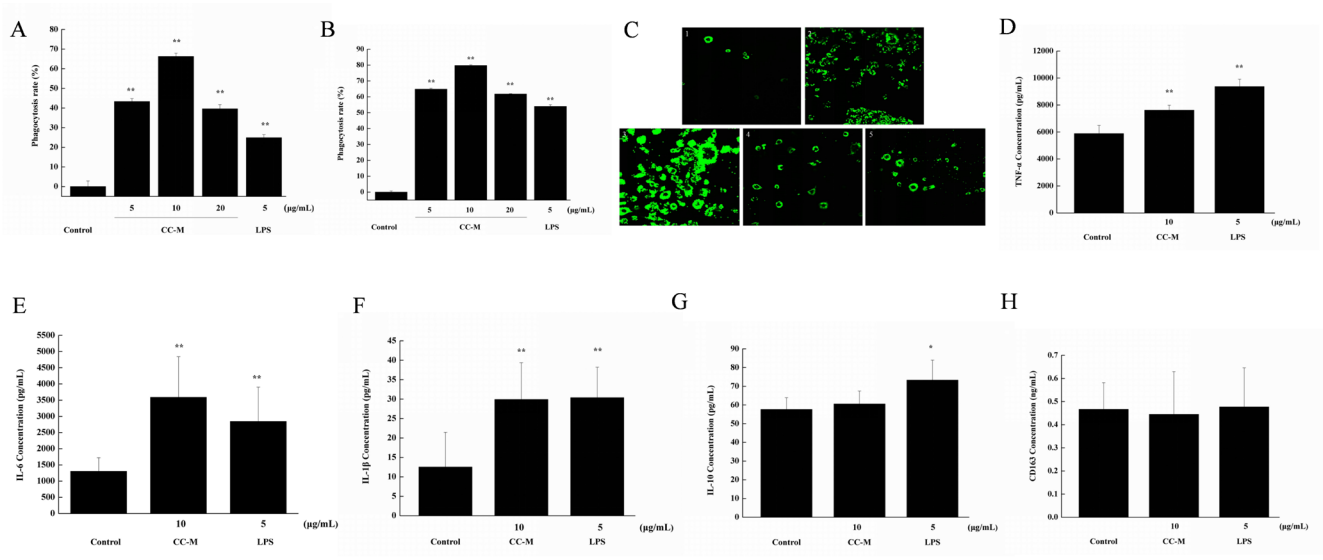


**Figure 4**. (A) Effect of CC-M on the ability of macrophages to phagocytose neutral red; (B) Effect of CC-M on the ability of macrophages to phagocytose fluorescent microspheres; (C) The cells morphology of RAW264.7 cells phagocytosing fluorescent microspheres under the action of CC-M; (D-H) The secretion of TNF-α, IL-6, IL-1β, IL-10and CD163 in RAW264.7 cells stimulated by CC-M; (I) Effect of CC-M on the expression of iNOS in RAW264.7. Compared with the control group, the difference was significant ($P < 0.05$) expressed by * and very significant ($P < 0.01$) expressed by **.

IL-6, IL-1 β, IL-10 and CD163 showed that the R value of the standard curve is greater than 0.99, which indicates that the fitting degree is excellent and the experimental results are reliable. The results of CC-M effect on the secretion of TNF-α, IL-6, IL-1 β, IL-10 and CD163 by RAW264.7 cells are shown in Figure 4D-4H. Polysaccharide CC-M of concentration of 10 μg/ml can promote the secretion of TNF-α, IL-6 and IL-1 β by RAW264.7 cells with a very significant difference compared with the blank control group ($P < 0.01$), but it can not promote the secretion of IL-10 and CD163 by RAW264.7 cells.

### *3.17 Quantitative analysis of gene expression*

In the screening of the two polysaccharides on the proliferation of immune cells, CC-M has a strong immune proliferation activity on RAW264.7 cells. Transcriptome analysis was done to explore the molecular mechanism of CC-M on RAW264.7 cells proliferation. After RNA-sequencing of RAW264.7 cells of control, CC-M and LPS groups, raw data (raw reads) were obtained, respectively. After removing the spliced reads and low-quality reads, 7.51 G (Control), 7.50 G (CC-M) and 7.91 G (LPS) analysis data (clean Reads) were obtained, respectively, in which Q20 (%) of each sample was greater than 97%, Q30 (%) was greater than 94%, GC content is about 50.00%, and base error rate was less than 0.03%. At the same time, the total alignment rates of control, CC-M and LPS groups were 92.05%, 92.18% and 93.87% respectively, which were all higher than 92%; the number of exons in the three groups accounted for 92.28%, 91.00% and 89.81% of the successful alignment, respectively. The above results show that the sequencing results were reliable and could be used for the next analysis and research.

The results of gene expression level analysis showed that there were 11 120 genes expressed in control group, accounting for 20.39% of the total genes; 11 162 genes expressed in CC-M group, accounting for 20.47% of the total genes; 11 502 genes expressed in LPS group, accounting for 21.09% of the total genes. Further analysis showed that there were 7 genes highly expressed in control group (FPKM > 2 000): *Lyz2*, *Fth1*, *MT-CO1*, *Eef1a1*, *Spp1*, *Rplp1* and *mt-Cytb*, 6 genes highly expressed in CC-M group (FPKM > 2 000): *Lyz2*, *Fth1*, *MT-CO1*, *Eef1a1*, *Spp1* and *Rplp1*, and 10 genes highly expressed in LPS group (FPKM > 2 000): *Lyz2*, *Fth1*, *MT-CO1*, *Eef1a1*, *Spp1*, *Rplp1*, *Ftl1*, *Actb*, *Ccl3* and *Cd14*, respectively. *Lyz2* encodes lysozyme 2 protein, and the high expression of *Lyz2* indicated that CC-M played an important role in antiviral, antibacterial and anti-inflammatory aspects. It is worth noting that *Eef1a1* is eukaryotic translation elongation factor 1 α1 (Soares & Abbott, 2013), and the expression level of *Eef1a1* in CC-M drug group and LPS group were lower than that in blank control group, suggesting that the protein activity in RAW264.7 cells has similar changes under the action of CC-M and LPS.

### *3.18 Differential gene analysis*

After quantitative analysis of gene expression, statistical analysis of gene expression data was carried out to screen the genes with significant expression differences in different samples under the same conditions. Based on the three biological repeats in this experiment, the significance of gene differential expression was analyzed by using DESeq2 software, and $|\log2(\text{foldchange})| > 0$ and $\text{Padj} < 0.05$ was used as the screening criteria. The results are shown in Figure 5A, 5B. Compared with the blank control group, the expression of 1 179 genes in CC-M

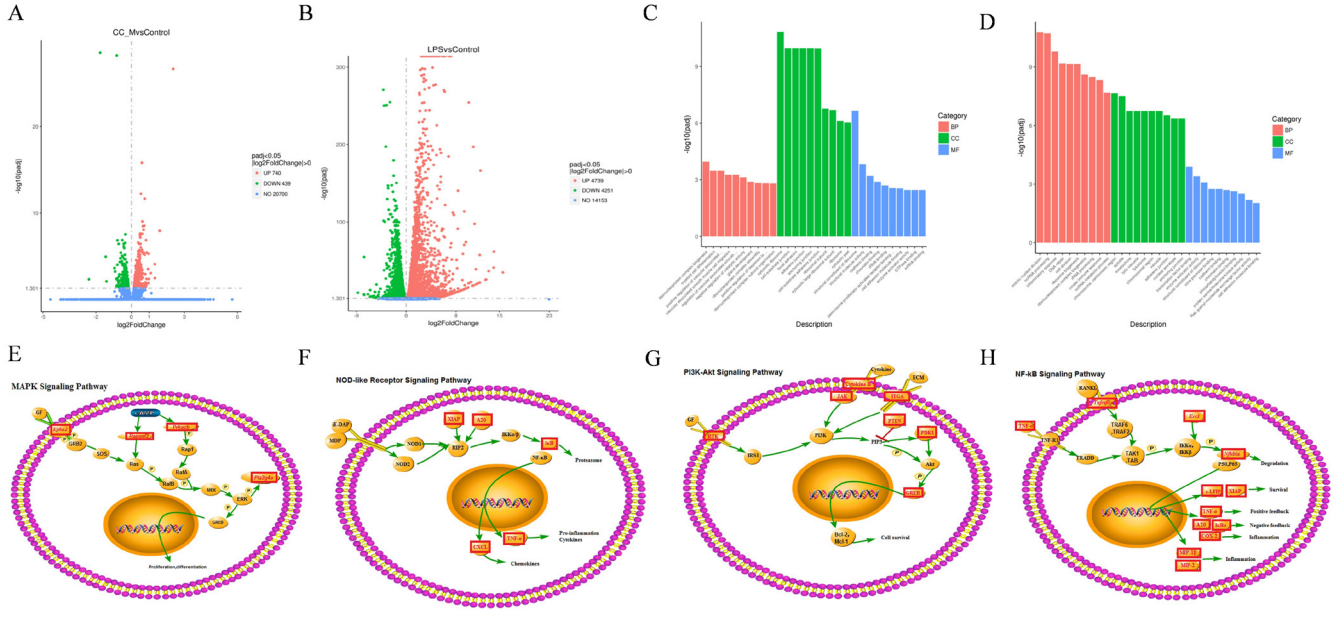


**Figure 5**. (A) Volcanic map analysis of differential gene expression of CC-M group compared with control group; (B) Volcanic map analysis of differential gene expression of LPS group compared with control group; (C) Classification and analysis of gene function of CC-M group compared with Control group; (D) Classification and analysis of gene function of LPS group compared with Control group; (E-H) The MAPK signaling pathway, NOD like receptor signaling pathway, PI3K-Akt signaling pathway and NF-κB signaling pathway in RAW264.7 cells stimulated by CC-M.

group was significantly different, including 740 up-regulated genes and 439 down regulated genes, among which the top ten up-regulated genes were: *Cxcl2, Gm17024*, *Csrnp1*, *Ptgs2*, *Gm43328*, *Gm5417*, *1700109H08Rik*, *Gm42664*, *Mss51* and *Lcor*; and the top ten down-regulated genes were *Gapdh*, *Hmgn2*, *Ddit4*, *Ighm*, *Gm8430*, *9330151L19Rik*, *2900052L18Rik*, *Gm26532*, *Txnip* and *Gm43980*. Meanwhile, the results show that a total of 8990 genes expressed in LPS compared with the blank control group have significant differences, including 4739 up-regulated genes and 4251 down-regulated genes, among which the top ten up-regulated genes were: *Il33*, *Csf3*, *Lcn2*, *Serpinb2*, *Urah*, *Il1f9*, *S100a8*, *Thbs1*, *Cxcl3* and *Il1a*; and the top ten down-regulated genes were: *Myadml2*, *Adgre4*, *Ighm*, *Siglech*, *Cd300c*, *Ighj4*, *Gm5086*, *Cd300lg*, *Galnt9* and *A430078G23Rik*.

*Cxcl2* encoded chemokine ligand 2 protein. Chemokines played an important role in controlling the directional migration of cells, and the occurrence of directional migration of immune cells played an important role in completion immune response (Heidemann et al., 2003). In addition, chemokines can make neutrophils enter the lung in acute inflammation, suggesting that neutrophils can stimulate the body's immunity by secreting high levels of angiogenic factors such as VEGF to promote angiogenesis under the stimulation of CC-M. *PTGS2* is an inducible isoenzyme gene of prostaglandin endoperoxide synthase PTGS , and its expression product is cyclooxygenase (COX-2) (Kunzmann et al., 2013). Cyclooxygenase is the rate limiting enzyme of prostaglandin synthesis, and prostaglandin is closely related to cell mitosis . The expression of *PTGS2* was up-regulated in CC-M group, which indicated that the mitotic activity of RAW264.7 cells was enhanced and the cell proliferation was accelerated under the stimulation of CC-M. *Mss51* encoded mitochondrial translation activator protein (Perez-Martinez, 2003), which is up-regulated in CC-M group, suggesting that CC-M plays an important role in maintaining muscle mitochondrial integrity and glucose metabolism in the process of cell proliferation. The results also showed that the up-regulated genes in RAW264.7 cells treated with LPS were different from those in the CC-M group, suggesting that the mechanism of CC-M promoting the proliferation of RAW264.7 cells was different from that of LPS.

### *3.19 Go enrichment analysis of differential genes*

Go enrichment analysis is to classify the function of different genes obtained by sequencing, and to know which branch they belong to: cellular component, molecular function and biological process, and the threshold value of significant enrichment was Padj < 0.05. The results showed that 1089 genes were successfully annotated in gene ontology, and these 1089 genes were enriched in 6048 Go gene categories. There were 356 GO genebanks in CC-M group, including 278 biological processes such as ribonucleoprotein complex biogenesis and intracellular receptor signaling pathway, 49 cellular components, including mitochondrial respiratory chain, 29 molecular functions, including structural constitution of ribosome and hydrogen ion transmembrane transporter activity. Further analysis showed that ribonucleoprotein complex biogenesis in biological process (BP), cytosolic ribosome in cellular component (CC) and structural construct of ribosome in molecular function (MF) were the most abundant Go gene categories (Figure 5C, 5D). At the same time, 8990 differentially expressed genes in LPS group were analyzed for Go enrichment. The results showed that a total of 7 667 genes were successfully annotated in gene ontology and enriched in 6 856 Go gene categories. The differential genes between LPS group and blank control group were significantly enriched in 877 Go gene categories, including 722 biological processes such as mitotic nuclear division, innate immune response, enzyme activator activity, and RAS guanyl nucleotide exchange factor activity etc. At the same time, mitotic nuclear division in biological process (BP), chromosomal central region in cellular component (CC) and transcription factor binding in molecular function (MF) are the most significant Go gene categories (Figure 5C, 5D). The results further indicate that the mechanism of CC-M and LPS stimulating RAW264.7 cell proliferation was different.

### *3.20 KEGG enrichment analysis of differential genes*

In this study, KEGG enrichment analysis was used to explore the different gene enrichment pathways of CC-M compared with blank control group and LPS group, and to explore the mechanism of CC-M affecting the activity of Raw254.7 cells. The results showed that 526 genes were enriched in 285 pathways among 1179 differential genes of CC-M compared with the blank control group. After excluding other disease-related pathways with different gene enrichment, CC-M group compared with blank control group has different gene enrichment in MAPK signaling pathway, NOD-like receptor signaling pathway, PI3K-Akt signaling pathway and NF-kappa B signaling pathway (Figure 5E-5H). Among the 8 990 differentially expressed genes in LPS group compared with the blank control group, 3 228 differentially expressed genes were enriched in 309 pathways.

MAPK signaling pathway is a common signal transduction mode inside and outside the nucleus, which can regulate cell proliferation, differentiation and apoptosis (Seger & Wexler, 2016). Compared with the blank control group, CC-M group had 24 differentially expressed genes enriched in MAPK signaling pathway, among which 16 genes were up-regulated, including *TNF*, *Rapgef2*, *Map3k2*, *Flnb, Pla2g4a*, *Taok3*, *Taok1*, *Flna*, *Epha2*, *Prkacb*, *Atf2, et al.*, and 8 genes were down regulated, including *Fos*, *Mapkapk2*, *Mapk3*, *Map3k11*, *Jund*, *Pdgfb*, *Vegfb* and *Taok2*. Tumor necrosis factor (TNF-α) encoded by TNF belongs to the tumor necrosis factor (TNF) superfamily. TNF-α is a proinflammatory factor with multiple functions , which plays an important role in innate immune response and regulation of internal environment balance (Dumitru et al., 2000). TNF-α can kill tumor cells, resist infection, induce the expression of IL-6, that indicated CC-M could activate JNK and p38 MAPK pathways, which participate in cell differentiation, proliferation and apoptosis. PLA2G4A protein can mediate the formation of arachidonic acid (Wei & Hemmings, 2004). Arachidonic acid is converted into intermediate products under the action of cyclooxygenase (COX-2), which is further metabolized into prostaglandins and other eicosanoic acids. These eicosanoic acids mediate many biological processes, including inflammation, development, reproduction, cellular immunity, cancer and energy homeostasis, suggesting that CC-M can promote cell

proliferation by up-regulating PLA2G4A to promote MAPK signaling pathway. Rasa1 and Rasa2 proteins are part of the Gap1 family of GTPase activating proteins (Boon et al., 2005). The up-regulated expression of these two genes suggests that CC-M can enhance the activity of Ras protein and control cell proliferation and differentiation. Dusp1, Dusp2 and Dusp4 are members of the DUSP family, which were considered to be a group of molecular designated control devices that regulate MAPK signaling (Shipp et al., 2010). The family genes are up-regulated in MAPK signaling pathway suggesting that CC-M can regulate the immune function and proliferation of RAW264.7 cells, and enhance the function of innate and adaptive immune effectors.

NF-κB signaling pathway plays an important role in the immune system through the production of cytokines, cyclooxygenase (COX-2) and growth factors, and plays an important role in maintaining the normal physiological function of the body (Vallabhapurapu & Karin, 2009). When NF-κB signaling pathway is activated, IκB will be degraded, which will induce the production of proinflammatory factors, chemokines and enzymes of secondary inflammatory mediators, such as TNF-α, Cxcl2 and COX-2. TNF-α can enhance the systemic inflammatory response and often induce the continuous production of PGE2 and other prostaglandins, which will increase the activation of NF-κB through positive feedback mechanism, and further increase the production of pro-inflammatory cytokines. In addition, TNF-α itself can activate NF-κB (p65-p50 dimer), further expanding the initial inflammatory response (Varfolomeev et al., 2008). In this study, there are 13 genes enriched in NF-κB signaling pathway, and all of them are up-regulated genes, including *Cxcl2, Nfkbia, Ptgs2, Tnfaip3* and *TNF*. These genes are up-regulated under the action of CC-M, suggesting that CC-M can activate NF-κB signaling pathway, which can produce pro-inflammatory factors and chemokines to play the role of inflammation, clear pathogens, and can up-regulate A20 protein to inhibit the body's excessive inflammatory response and maintain the body's balance.

PI3K-Akt signaling pathway is related to cell proliferation and differentiation. Studies have shown that PI3K-Akt signaling pathway is related to osteoclast generation (Luo et al., 2003), and plays an important role in cell proliferation, growth and metabolism, and can cause the immune response of RAW264.7 cells. When cytokines bind to the receptors on the cell membrane, the downstream JAK kinase family is activated, and then PI3K is activated, which can catalyze the formation of PIP3. As a second messenger, PIP3 activates Akt, which regulates downstream molecules including GREB to ensure cell survival (Luo et al., 2003). There were 18 genes enriched in PI3K-Akt signaling pathway, 12 of which were up-regulated, including *Jak2, Gsk3b, Pdpk1, Pten*, et al. and 6 of which were down regulated, including *Didt4, Lpar6, Mapk3, Pdgfb,* et al. These results suggest that CC-M can ensure cell survival by up regulating JAK kinase family genes. At the same time, PTEN gene is up-regulated to inhibit excessive cell proliferation through negative regulation, so as to maintain cell and body homeostasis.

NOD like receptor is a pattern recognition receptor (PRR), which consists of five subfamilies, namely NLRA, NLRB, NLRC, NLRP and NLRX. NLRC and NLRP are the main subfamilies of nod like receptor, while NOD1 and NOD2 of NLRC subfamily are the most widely studied and representative proteins (Castaño-Rodríguez et al., 2014). Both bacteria and viruses can activate the nod like receptor signaling pathway. In general, when bacteria invade cells, NOD1 and NOD2 can recognize the iE DAP and MDP of bacteria, and activate the NOD like receptor. The activated NOD like receptor can recruit factors related to the activation of IKK /IKKβ, such as RIP2, IAP, CIAP, XIAP and TAK1, which activate the transcription of NF-κB and promote the release of IL-1β, TNF-α and IL-6 (33). In addition, after activation of NOD like receptor, it can also recruit downstream CARD9, thus activating p38 and JNK, finally activating MAPK pathway, promoting the release of TNF-α and chemokine CXCL. In this study, there were 20 differentially expressed genes in NOD like receptor signaling pathway, 13 of which were up-regulated, including *Cxcl2*, *Nfkbia*, *TNF*, *Xiap*, *Tnfaip3*, r\et al. and 7 of which were down-regulated, including *Txnip*, *Irf3*, *Mpk3*, et al. Under the stimulation of CC-M, *Xiap* and *Tnfaip3* were up-regulated, which suggested that the activation of NOD receptor activated RIP2 by recruiting XIAP and TNFAIP3 downstream, and then activated NF-κB and MAPK signaling pathways, promoting the release of TNF - α and chemokine Cxcl2.

## 4 Conclusion

In this study, hot water extraction, ethanol precipitation, DEAE-52 cellulose and column chromatography were used to extract and purify the crude polysaccharides of *Craterellus cornucopioide* and *Dictyophora indusiata (Vent.ex Pers) Fisch*. Two new polysaccharides were extracted from the fruiting bodies of *Craterellus cornucopioide* and *Dictyophora indusiata (Vent.ex Pers) Fisch,* respectively. The results showed that the molecular weight of *Craterellus cornucopioide* polysaccharide (CC-M) was 20 482 Da, and that of *Dictyophora indusiata (Vent.ex Pers) Fisch* (DI-Z) was 9 779 Da. The results of structure identification by GC-MS, HPGPC, HPLC, FT-IR and NMR showed that CC-M was composed of Xyl: Glc: Gal in a ratio of 2:5:4. The CC-M takes 1,6-glucose and 1,6-galactose as skeletons, extends a branched chain from galactose 2-O to connect 1,3,4-xylose, and connects β-4-glucose terminal monosaccharide to xylose. DI-Z was also composed of Xyl: Glc: Gal in the ratio of 2:6:5. In accordance with FT-IR, monosaccharide composition and methylation results of DI-Z, it was inferred that DI-Z takes 1,6-glucose and 1,6-galactose as skeletons, extends a branched chain from galactose 2-O to connect 1,4-xylose and β-4-glucose as terminal group. By comparing the fine structure of CC-M and DI-Z, it was found that CC-M has larger molecular weight, more branch chains and better water solubility. The results of immunoactivity showed that CC-M and DI-Z have the proliferation activity of B cells, T cells and RAW264.7 cells in vitro, and the effect of CC-M on the proliferation of immune cells was higher than that of DI-Z. In addition, CC-M could significantly promote the secretion of TNF - α, IL-6, IL-1 β, IL-10 and CD163 and enhance the phagocytic ability of RAW264.7 cells. Western blot results showed that CC-M promoted RAW264.7 cells to M1 polarization. The results of RNA-sequencing showed that CC-M exerted its proliferative activity and immunoregulatory activity on RAW264.7 cells through the interaction of MAPK signaling pathway, NOD like receptor signaling pathway, PI3K-Akt signaling pathway and NF-κB signaling pathway. In conclusion,

CC-M and DI-Z were both natural polysaccharides with novel structure, which had immune and proliferationactivity for specific immune cells. To explore the structure of *Craterellus cornucopioide* polysaccharide (CC-M) and *Dictyophora indusiata (Vent.ex Pers) Fisch* polysaccharide (DI-Z) and the structure-activity relationship between them can provide a better theoretical basis for the research and development of medicinal value of CC-M and DI-Z.

## Availability of data and material

The datasets used and/or analyzed during the current study are available from the corresponding author on reasonable request.

## Funding

This project was supported by the Open Project Program of Irradiation Preservation Technology Key Laboratory of Sichuan Province, Sichuan Institute of Atomic Energy (FZBC2020009), the Science and Technology Support Project of Sichuan Province (2018JY0087 and 2018NZ0055), Science and Technology Support Project of Nanchong science and Technology Bureau of Sichuan Province (20YFZJ0053).

## Author contributions

Yiling Hou conceived and designed the experiments of the present study. Xiang Ding, Miao Zhu and Yiling Hou performed the experiments and acquired data. Xiang DING and Yiling HOU drafted the manuscript and revised it critically. All authors read and approved the final manuscript.

## References

Boon, L. M., Mulliken, J. B., & Vikkula, M. (2005). RASA1: variable phenotype with capillary and arteriovenous malformations. *Current Opinion in Genetics & Development*, 15(3), 265-269. http://dx.doi.org/10.1016/j.gde.2005.03.004. PMid:15917201.

Brown, J., Martinez, O. I., & Melton, D. A. (2004). Adult pancreatic β-cells are formed by self-duplication. *Nature*, 429, 41-46. http://dx.doi.org/10.1038/nature02520. PMid:15129273.

Castaño-Rodríguez, N., Kaakoush, N. O., Goh, K. L., Fock, K. M., & Mitchell, H. M. (2014). The NOD-Like receptor signalling pathway in helicobacter pylori infection and related gastric cancer: a case-control study and gene expression analyses. *PLoS One*, 9(6), e98899. http://dx.doi.org/10.1371/journal.pone.0098899. PMid:24901306.

Chihara, G., Maeda, Y., Hamuro, J., Sasaki, T., & Fukuoka, F. (1969). Inhibition of mouse sarcoma 180 by polysaccharides from lentinus edodes (berk.) sing. *Nature*, 222, 687-688. http://dx.doi.org/10.1038/222687a0. PMid:5768289.

Cock, P. J. A., Fields, C. J., Goto, N., Heuer, M. L., & Rice, P. M. (2010). The Sanger FASTQ file format for sequences with quality scores, and the Solexa/Illumina FASTQ variants. *Nucleic Acids Research*, 38(6), 1767-1771. http://dx.doi.org/10.1093/nar/gkp1137. PMid:20015970.

Ding, X., Hou, Y. L., & Hou, W. R. (2012a). Structure elucidation and antioxidant activity of a novel polysaccharide isolated from *Boletus speciosus Forst*. *International Journal of Biological Macromolecules*, 50(3), 613-618. http://dx.doi.org/10.1016/j.ijbiomac.2012.01.021. PMid:22285986.

Ding, X., Hou, Y. L., & Hou, W. R. (2012b). Structure feature and antitumor activity of a novel polysaccharide isolated from *Lactarius deliciosus Gray*. *Carbohydrate Polymers*, 89(2), 397-402. http://dx.doi.org/10.1016/j.carbpol.2012.03.020. PMid:24750736.

Du, B., Fu, Y., Wang, X., Jiang, H., Lv, Q., Du, R., Yang, Y., & Rong, R. (2019). Isolation, purification, structural analysis and biological activities of water-soluble polysaccharide from *Glehniae radix*. *International Journal of Biological Macromolecules*, 128, 724-731. http://dx.doi.org/10.1016/j.ijbiomac.2019.01.159. PMid:30703419.

Dumitru, C. D., Ceci, J. D., Tsatsanis, C., Kontoyiannis, D., Stamatakis, K., Lin, J. H., Patriotis, C., Jenkins, N. A., Copeland, N. G., Kollias, G., & Tsichlis, P. N. (2000). TNF-α induction by LPS is regulated posttranscriptionally via a Tpl2/ERK-dependent pathway. *Cell*, 103(7), 1071-1083. http://dx.doi.org/10.1016/S0092-8674(00)00210-5. PMid:11163183.

Evans, W. E., & McLeod, H. L. (2003). Pharmacogenomics-drug disposition, drug targets, and side effects. *The New England Journal of Medicine*, 348(6), 538-549. http://dx.doi.org/10.1056/NEJMra020526. PMid:12571262.

Goodridge, H. S., Wolf, A. J., & Underhill, D. M. (2009). Beta-glucan recognition by the innate immune system. *Immunological Reviews*, 230(1), 38-50. http://dx.doi.org/10.1111/j.1600-065X.2009.00793.x. PMid:19594628.

Guo, M., Meng, M., Duan, S., Feng, C., & Wang, C. (2019). Structure characterization, physicochemical property and immunomodulatory activity on RAW264.7 cells of a novel triple-helix polysaccharide from *Craterellus cornucopioides*. *International Journal of Biological Macromolecules*, 126, 796-804. http://dx.doi.org/10.1016/j.ijbiomac.2018.12.246. PMid:30594621.

Habtemariam, S. (2019). The chemistry, pharmacology and therapeutic potential of the edible mushroom *dictyophora indusiata* (*Vent* ex. *Pers.*) Fischer (Synn. *Phallus indusiatus*). *Biomedicines*, 7(4), 98-119. http://dx.doi.org/10.3390/biomedicines7040098. PMid:31842442.

Hanahan, D., & Weinberg, R. A. (2000). The hallmarks of cancer. *Cell*, 100(1), 57-70. http://dx.doi.org/10.1016/S0092-8674(00)81683-9. PMid:10647931.

Heidemann, J., Ogawa, H., Dwinell, M. B., Rafiee, P., Maaser, C., Gockel, H. R., Otterson, M. F., Ota, D. M., Lugering, N., Domschke, W., & Binion, D. G. (2003). Angiogenic effects of interleukin 8 (CXCL8) in human intestinal microvascular endothelial cells are mediated by CXCR2. *The Journal of Biological Chemistry*, 278(10), 8508-8515. http://dx.doi.org/10.1074/jbc.M208231200. PMid:12496258.

Kamnev, A. A., Tugarova, A. V., Dyatlova, Y. A., Tarantilis, P. A., Grigoryeva, O. P., Fainleib, A. M., & Luca, S. (2018). Methodological effects in Fourier Transform Infrared (FTIR) spectroscopy: implications for structural analyses of biomacromolecular samples. *Spectrochimica Acta. Part A, Molecular and Biomolecular Spectroscopy*, 193, 558-564. http://dx.doi.org/10.1016/j.saa.2017.12.051. PMid:29310090.

Korfage, I. J., Koning, H. J. D., Habbema, J. D. F., Schröder, F. H., & Essink-Bot, M. L. (2007). Side-effects of treatment for localized prostate cancer: are they valued differently by patients and healthy controls? *BJU International*, 99(4), 801-806. http://dx.doi.org/10.1111/j.1464-410X.2006.06707.x. PMid:17233804.

Kumar, M. N. V. R. (2000). A review of chitin and chitosan applications. *Reactive & Functional Polymers*, 46(1), 1-27. http://dx.doi.org/10.1016/S1381-5148(00)00038-9.

Kunzmann, A. T., Murray, L. J., Cardwell, C. R., McShane, C. M., McMenamin, U. C., & Cantwell, M. M. (2013). PTGS2 (Cyclooxygenase-2) expression and survival among colorectal cancer patients: a systematic review. *Cancer Epidemiology, Biomarkers & Prevention*, 22(9), 1490-1497. http://dx.doi.org/10.1158/1055-9965.EPI-13-0263. PMid:23810915.

Leeuwen, S. S., Kuipers, B. J. H., Dijkhuizen, L., & Kamerling, J. P. (2014). Development of a 1H NMR structural-reporter-group

concept for the analysis of prebiotic galacto-oligosaccharides of the [β-d-Galp-(1→x)]n-d-Glcp type. *Carbohydrate Research*, 400, 54-58. http://dx.doi.org/10.1016/j.carres.2014.08.011. PMid:25249391.

Luo, J., Manning, B. D., & Cantley, L. C. (2003). Targeting the PI3K-Akt pathway in human cancer: rationale and promise. *Cancer Cell*, 4(4), 257-262. http://dx.doi.org/10.1016/S1535-6108(03)00248-4. PMid:14585353.

Perez-Martinez, X., Broadley, S. A., & Fox, T. D. (2003). Mss51p promotes mitochondrial Cox1p synthesis and interacts with newly synthesized Cox1p. *The EMBO Journal*, 22(21), 5951-5961. http://dx.doi.org/10.1093/emboj/cdg566. PMid:14592991.

Ramberg, J. E., Nelson, E. D., & Sinnott, R. A. (2010). Immunomodulatory dietary polysaccharides: a systematic review of the literature. *Nutrition Journal*, 9(1), 54. http://dx.doi.org/10.1186/1475-2891-9-54. PMid:21087484.

Seger, R., & Wexler, S. (2016). The MAPK signaling cascades. Encyclopedia of Cell Biology, 3, 122-127.

Shipp, L. E., Lee, J. V., Yu, C. Y., Pufall, M., Zhang, P., Scott, D. K., & Wang, J. C. (2010). Transcriptional regulation of human Dual Specificity Protein Phosphatase 1 (DUSP1) gene by glucocorticoids. *PLoS One*, 5(10), e13754. http://dx.doi.org/10.1371/journal.pone.0013754. PMid:21060794.

Soares, D. C., & Abbott, C. M. (2013). Highly homologous eEF1A1 and eEF1A2 exhibit differential post-translational modification with significant enrichment around localised sites of sequence variation. *Biology Direct*, 8, 29. http://dx.doi.org/10.1186/1745-6150-8-29. PMid:24220286.

Su, S., Ding, X., Fu, L., & Hou, Y. (2019). Structural characterization and immune regulation of a novel polysaccharide from Maerkang Lactarius deliciosus Gray. *International Journal of Molecular Medicine*, 44(2), 713-724. http://dx.doi.org/10.3892/ijmm.2019.4219. PMid:31173162.

Vallabhapurapu, S., & Karin, M. (2009). Regulation and function of NF-κB transcription factors in the immune system. *Annual Review of Immunology*, 27(1), 693-733. http://dx.doi.org/10.1146/annurev.immunol.021908.132641. PMid:19302050.

Varfolomeev, E., Goncharov, T., Fedorova, A. V., Dynek, J. N., Zobel, K., Deshayes, K., Fairbrother, W. J., & Vucic, D. (2008). c-IAP1 and c-IAP2 are critical mediators of tumor necrosis factor α (TNFα)-induced NF-κB activation. *The Journal of Biological Chemistry*, 283(36), 24295-24299. http://dx.doi.org/10.1074/jbc.C800128200. PMid:18621737.

Wei, J., & Hemmings, G. P. (2004). A study of a genetic association between the PTGS2/PLA2G4A locus and schizophrenia. *Prostaglandins, Leukotrienes, and Essential Fatty Acids*, 70(4), 413-415. http://dx.doi.org/10.1016/j.plefa.2003.12.018. PMid:15041036.

Yang, W. W., Wang, L. M., Gong, L. L., Lu, Y. M., Pan, W. J., Wang, Y., Zhang, W. N., & Chen, Y. (2018). Structural characterization and antioxidant activities of a novel polysaccharide fraction from the fruiting bodies of Craterellus cornucopioides. *International Journal of Biological Macromolecules*, 117, 473-482. http://dx.doi.org/10.1016/j.ijbiomac.2018.05.212. PMid:29857101.

Yeo, S. J., Yoon, J. G., Hong, S. C., & Yi, A. K. (2003). Cpg dna induces self and cross-hyporesponsiveness of raw264.7 cells in response to cpg dna and lipopolysaccharide: alterations in il-1 receptor-associated kinase expression. *Journal of Immunology*, 170(2), 1052-1061. http://dx.doi.org/10.4049/jimmunol.170.2.1052. PMid:12517973.

Zheng, W. P., & Flavell, R. A. (2016). The transcription factor gata-3 is necessary and sufficient for th2 cytokine gene expression in cd4 T cells. *Journal of Immunology*, 196(11), 4426-4435. PMid:27207805.